MechSE

CCC Annual Report

UIUC, August 20, 2014

Effect of EMBr on Flow and Particle Capture and Parametric Studies of Transient Flow with LES on GPU

Kai Jin

Department of Mechanical Science & Engineering
University of Illinois at Urbana-Champaign

Outline

- Multi-GPU CUFLOW development
- Parametric study: LES simulations of effect of EMBr on fluid flow in the mold at different casing speed
- Validation of particle capture criterion
- Effect of magnetic field on particle capture

Configuration of BWs XK node and Our Lab Workstation

Currently, two versions of CUFLOW, CPU and GPU versions:

- CPU version, run on multi-CPU PC (data compunication through MPI)
- GPU version, run on multi-GPU PC and multi-CPU&GPU pair supercomputer (eg. Blue Waters)

	PC - 4GPU Workstation	Blue Waters Supercomputer
#of Nodes	1	4224
Node CPU	Xeon E5-2650v2 Ivy Bridge, 2.60 GHz, 8 cores	AMD 6276, 2.3 GHz, 16 cores
GPU/Node	4 × Nvidia Tesla C2075, 4 × **5 GB**, 575 MHz	1 × Nvidia Tesla K20x, 1 × **6 GB**, 732 MHz

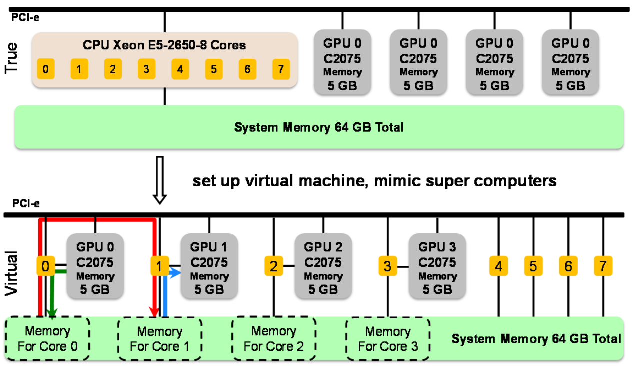

Configuration of 4GPU Workstation

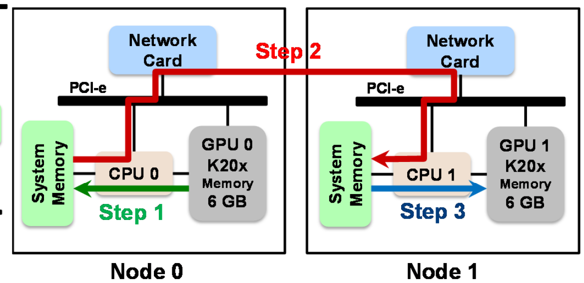

Three Steps: cudaMemcpy(...), MPI_Send(...) and MPI_Recv(...), cudaMemcpy(...)

Configuration of BWs Nodes (showing 2 nodes)

Validation 1 - Problem Setup

- Problem Setup: 3D lid-driven Cavity Flow, Re = 1000, on 4 GPUs
- Grid dimensions: **256×256×256** total ~**16.8 million** cells
- Multigrid: geometric multigrid with 6 grid levels
- Geometry: Unit Cube
- Boundary Conditions: no-slip wall; top lid velocity U_0 in z direction

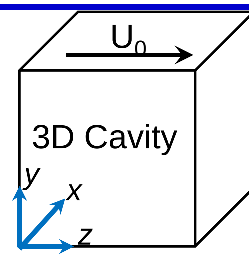

Domain decomposition, uniformly decomposed in z direction, as below:

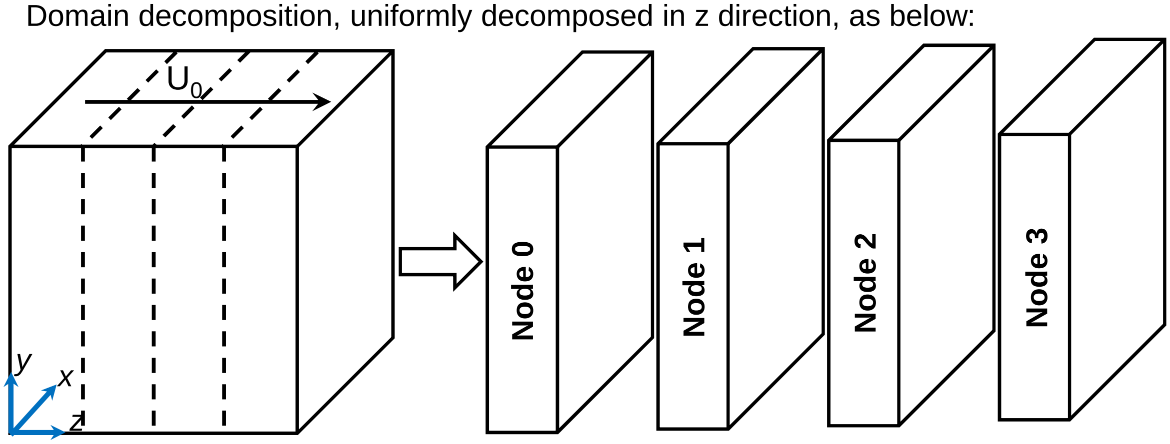

Validation - 1 Results

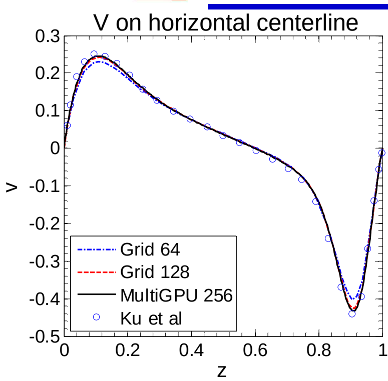

- For this 16.8 million cells, 4 GPUs, 0.678s/timestep, takes about ~18 hours to simulate 100 sec flow time.
- Velocities in symmetry plane of 4-GPU simulation (256^3) match exactly with single GPU results with different mesh refinements, (64^3, 128^3) and with previous work Ku et al*

***Ku, H.S., Hirsh, R.S., and Taylor, T.D., "A Psuedo-Spectral Method for Solution of the Three-Dimensional Incompressible Navier-Stokes Equations," J. of Computational Physics, Vol. 70, 1987, p. 439.**

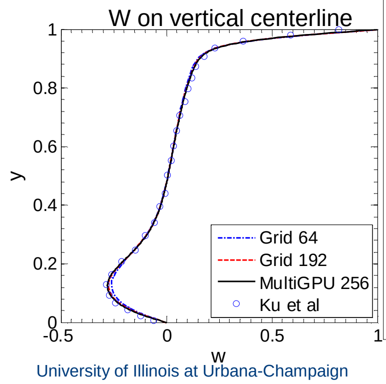

Streamlines in Symmetry Plane

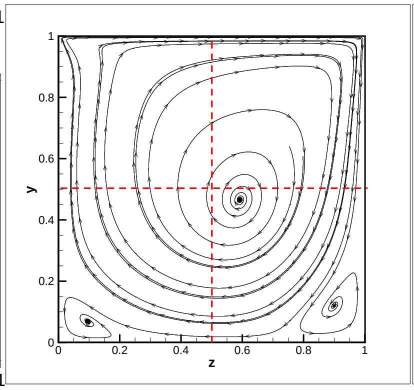

Contour of v in Symmetry Plane

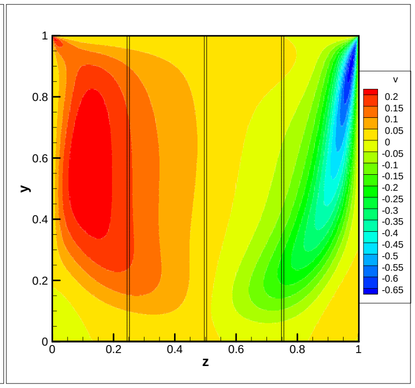

Validation 2 – Variable Viscosity Validation

- Lid-Driven Cavity Flow, Re=100, power-law behavior index is 0.5 (shear thinning fluid), using 4 GPUs.
- A uniform grid of **128×128×512 ~ 8.4** million cells, using 7 level multigrid, 5 sweeps and 5 V-cycles
- Geometry, cuboidal with dimension x:y:z = 1:1:4.
- Boundary Conditions: no slip wall; y=1 wall moving with speed U_0 in x direction;
- Assume boundary effect is negligible, the velocity on symmetry plane is compared with available 2D results (Because no 3D validation results available in literature).

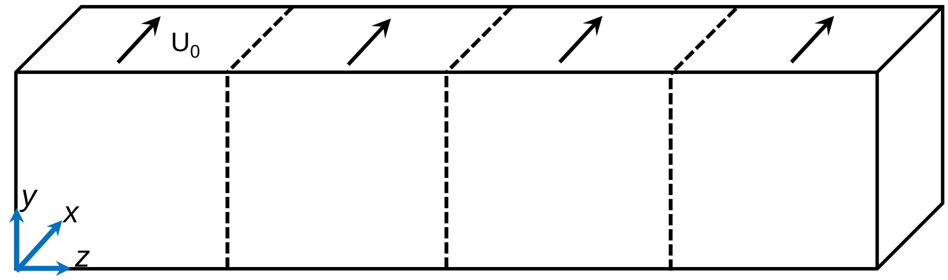

Validation 2 – Results Non-Newtonian Module Validation

- Centerline velocities are compare with published results [1-4] and our old CUFLOW validation run (same setup, same grid size).
- Timing: old CULFOW, 1GPU 1.41s/timesetp, new CUFLOW on 4 GPUs, 0.34 s/timestep, **speedup compare with old 1GPU CUFLOW is 4.14** (great than 4 because some data structure improvement, the memory access is more efficient)

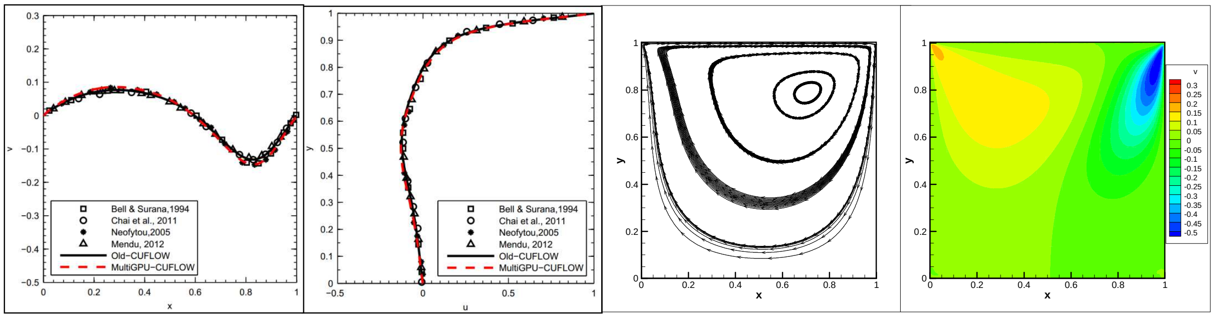

1. Bell, B.C. and Surana, K. S. "p-Version Least Squares Finite Element Formulation for Two-Dimensional, Incompressible, Non-Newtonian Isothermal and Non-Isothermal Fluid Flow," International J. for Num. Methods in Fluids, Vol. 18, pp. 127-162.
2. Neofytou, P. "A Third-Order Upwind Finite Volume Method for Generalized Newtonian Fluid Flows," Advances in Engineering Software, Vol. 36, 2005, pp. 664-680.
3. Chai, Z., et al. "Multiple-Relaxation-Time Lattice Boltzmann Model for Generalized Newtonian Fluid Flows," Journal of Non-Newtonian Fluid Mechanics, Vol. 166, 2011, pp. 332-342.
4. Mendu, S. S. and Das, P. K., "Flow of Power-Law Fluids in a Cavity Driven by the Motion of Two Facing Lids – a Simulation by Lattice Boltzmann Method." Journal of Non-Newtonian Fluid Mechanics, Vol. 175, 2012, pp. 10-24.

Speed Up and Comparison of BlueWaters XK Node and Our 4GPU Workstation

CUFLOW on BWs XK node and 4GPU WorkStation
3D Lid-Driven Cavity **128×128×512~8.4million cells**

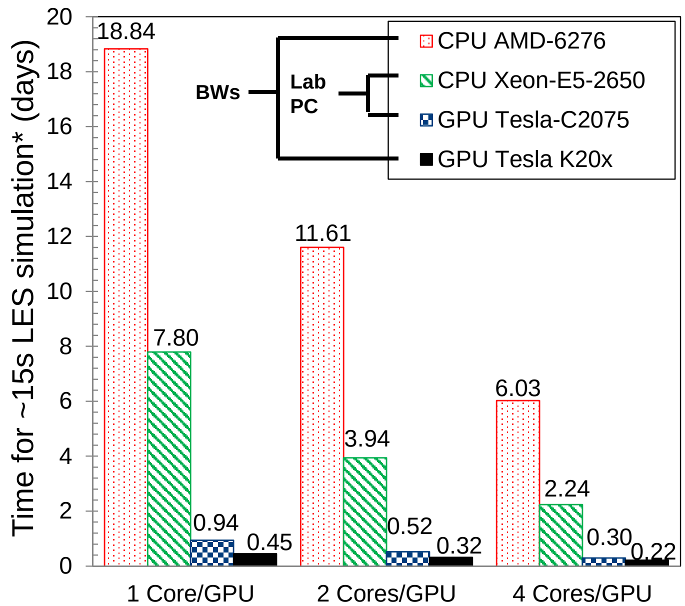

- Lab CPU is ~2.5 times faster than BW CPU;
- Tesla K20x is ~1.5-2.0 times faster than Tesla C2075;
- On BWs, 1 GPU vs. serial run on 1 core speed up is ~42x;
- One BWs XK node, 1 GPU is 13.4x faster than 4 CPU parallel execution;
- FLUENT, same problem one core on BWs estimated to be ~190 days which is 633 times slower than CUFLOW 4GPU parallel run on our Lab PC; but FLUENT with parallel run using all 32 cores in one BW XE node will make it 6 days which means ~20 times slower (assuming FLUENT has perfect scaling) than CUFLOW 4GPU runs on lab PC;

Part II - LES simulations of Effect of EMBr on Fluid Flow in the Mold at different Casing Speed

Objectives

- Use the new multi-GPU code to investigate the effect of EMBr on fluid flow in Baosteel caster with different casting speed, then study transient flow behavior in mold and level fluctuations at meniscus region and provide suggestions regarding operation.

Geometry, mesh and BCs

- Full-mold domain with SEN:
  176×32×800 = ~4.5million cells, uniform grid.

	Dimension (mm)	Cell Size (mm)
Lx – Mold Thickness	230	$\Delta x = 7.67$
Ly – Mold Width	1300	$\Delta y = 7.47$
Lz – Domain Length	6000	$\Delta z = 7.50$

- Boundary Conditions:
  - SEN top: velocity inlet;
  - Bottom: zero derivative of velocity;
  - WF and NF: moving downward with casting speed (no shell);
  - Top surface and walls: no penetration and no slip.

- Note the SEN inlet area is the “eye-shaped” intersected region of two circles to include the slide gate.

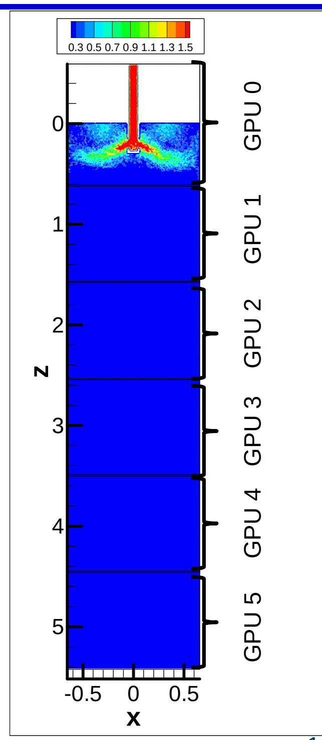

Parametric Study – Case Conditions

Mold Thickness 230mm and Width 1300mm; SEN Downward angle 15°

	Casting Speed Vc (m/min)	Submergence Depth (mm)	EMBr Top Coil Current (A)	EMBr Bottom Coil Current (A)
1	1.5	210	-	-
2	1.5	160	-	-
3	1.5	160	0	600
4	1.5	160	0	850
5	1.5	160	400	600
6	1.8	160	-	-
7	1.8	160	0	850
8	1.8	160	400	600

Measured and Applied Magnetic Field

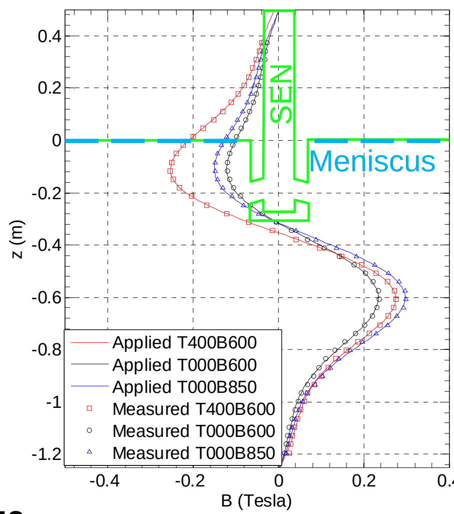

- All use **6 GPUs**;
- Initial velocity = zero, **timestep** is **0.0002s**;
- Simulated **42s** for all cases, allow **12s** for flow to **develop**;
- Time-averaged results are performed from **12s to 42s**, sample frequency **25Hz (data saved every 0.04s)**;

Magnetic Field: equations (curve fit of measurements)

T400 / B600 (z=0 at meniscus), -1.25<z<0.5, other places 0, Unit z(m) and B(Tesla)

B = 0.005651+(-0.1761)*cos(z*3.497)+(-0.06336)*sin(z*3.497)+(-0.06226)*cos(2*z*3.497)+0.08456*sin(2*z*3.497)+0.02178*cos(3*z*3.497)+0.02742*sin(3*z*3.497)

T000 / B600 (z=0 at meniscus), -1.25<z<0.5, other places 0, Unit z(m) and B(Tesla)

B = 0.029730+(-0.1158)*cos(z*3.582)+(-0.06543)*sin(z*3.582)+(-0.03495)*cos(2*z*3.582)+0.05917*sin(2*z*3.582)+0.02027*cos(3*z*3.582)+0.01087*sin(3*z*3.582)

T000 / B850 (z=0 at meniscus), -1.25<z<0.5, other places 0, Unit z(m) and B(Tesla)

B = 0.038420+(-0.1458)*cos(z*3.586)+(-0.08316)*sin(z*3.586)+(-0.04366)*cos(2*z*3.586)+0.07488*sin(2*z*3.586)+0.02564*cos(3*z*3.586)+0.01328*sin(3*z*3.586)

Governing Equations and Steel Properties

- Continuity Equation $\nabla \cdot \vec{u} = 0$
- Momentum equation (LES Coherent-structure Smagorinsky (CSM) Model)

$$\rho \left[\frac{\partial \vec{u}}{\partial t} + \left(\vec{u} \cdot \nabla \right) \vec{u} \right] = \nabla p + \left(\mu + \mu_{sgs} \right) \nabla^2 \vec{u} + \vec{F}$$

- MHD Equations – Potential Method

$$\vec{F} = \vec{J} \times \vec{B}_0 \qquad \nabla^2 \Phi = \nabla \cdot \left(\vec{u} \times \vec{B}_0 \right)$$

$$\vec{E} = -\nabla \Phi \qquad \vec{J} = \sigma \left(\vec{E} + \vec{u} \times \vec{B}_0 \right)$$

$$\nabla \cdot \vec{J} = 0$$

Properties of Steel	
Density (kg/m^3)	7,000
Viscosity (kg/m-s)	0.0063
Electrical Conductivity (S/m)	714,000
Magnetic Permeability (h/m)	1.26*10^{-6}

$\vec{u}$	Steel velocity
ρ	Steel density
μ	Steel viscosity
μ_{sgs}	Sub-grid scale viscosity
t	Time
p	Pressure
$\vec{E}$	Electric Field
$\vec{B}_0$	Megnetic Field
Φ	Electric Potential
$\vec{F}$	Megnetic Force
σ	Electric Conductivity

Effect of Submergence Depth On Velocity (Simulations 1 and 2) (no EMBr, Vc=1.5m/min)

- Velocity magnitude contours at center plane (m/s)
- **Deeper** submergence has slightly (**~5%**) **higher** surface velocity.

Submergence Depth *210mm*

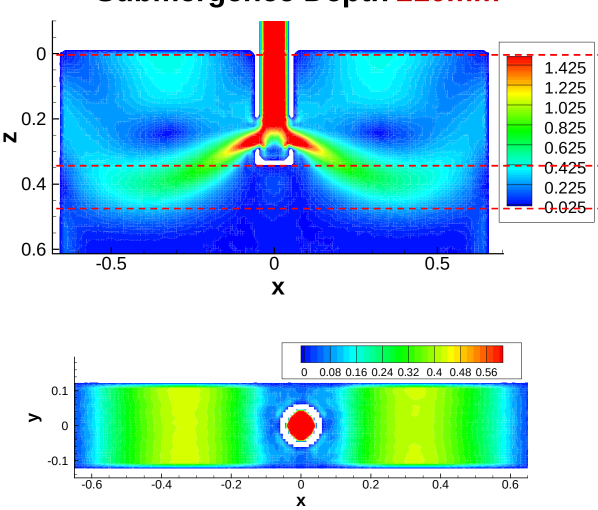

Submergence Depth *160mm*

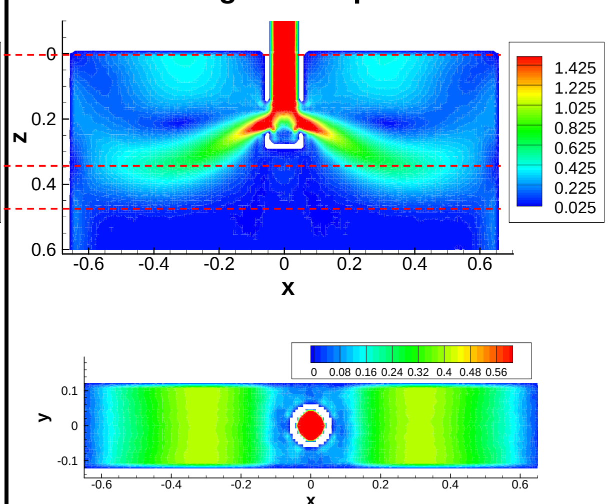

Max top surface velocity: ~0.43m/s **Max top surface velocity: ~0.41m/s**

Effect of EMBr (Simulations 2 to 5) (160mm Submergence, Vc = 1.5m/min)

- Velocity magnitude contours at center plane (m/s)
- Bottom EMBr only surface velocity reduced by ~67%, both top and bottom top surface velocity reduced by ~90%

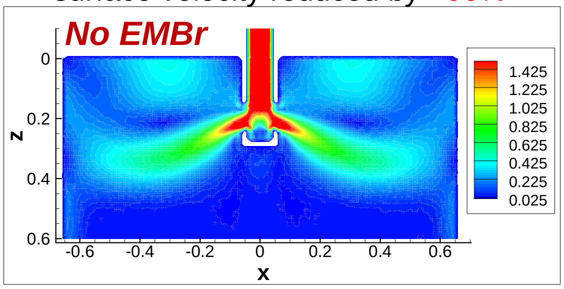

Max. top surface velocity: ~0.41m/s

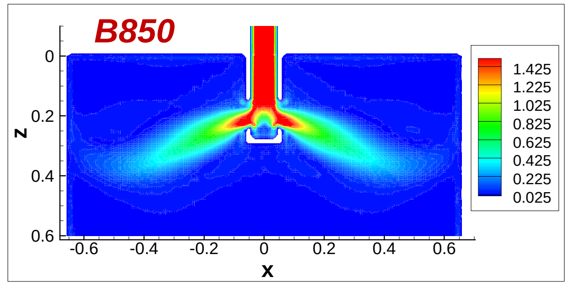

Max. top surface velocity: ~0.13m/s

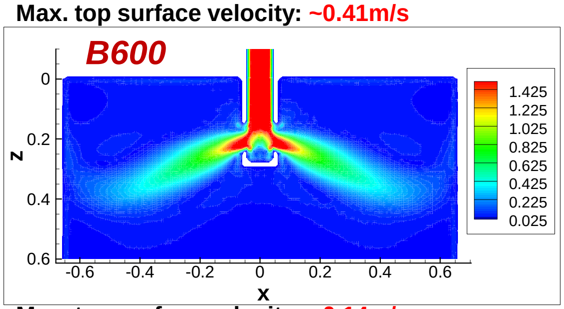

Max. top surface velocity: ~0.14m/s

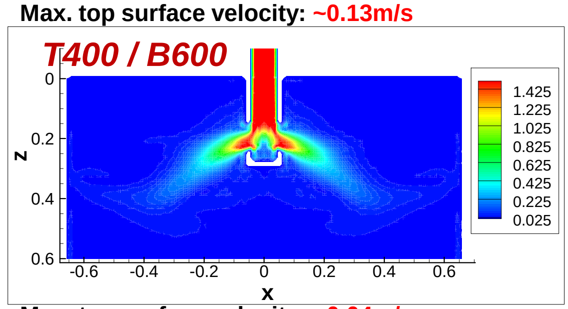

Max. top surface velocity: ~0.04m/s

Top Surface Time Averaged Velocity Magnitude for All Cases (Simulations 1 to 8)

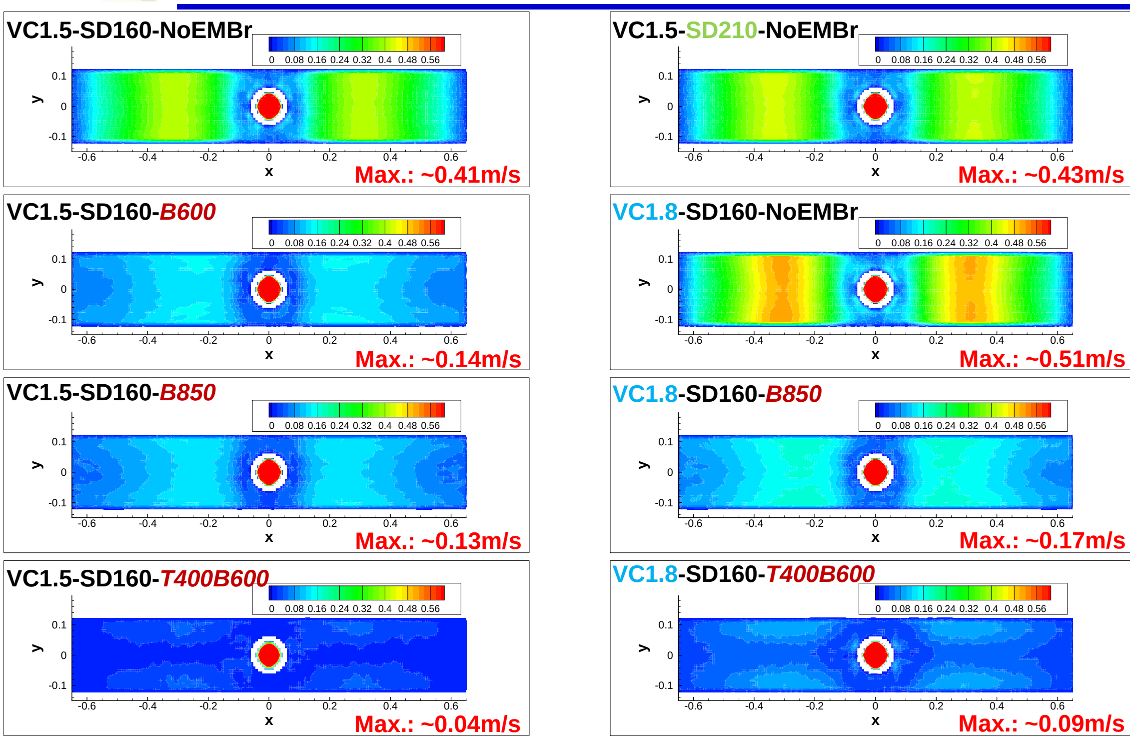

Effect of EMBr on Transient flow in Mid and Top Surfaces (160mm Submergence, Vc = 1.8m/min) (Simulations 6 and 7)

- Transient animation, contour of velocity magnitude (m/s)
- Top surface velocity reduced by **~67%** with bottom coil current 850A

VC1.8m/min-SD160mm-*NoEMBr*

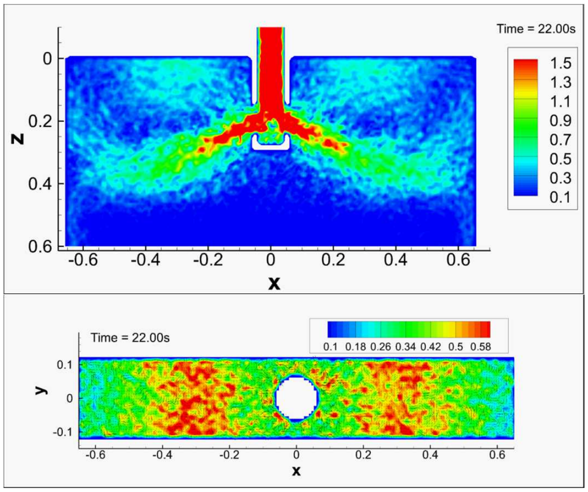

Time averaged Max top surface velocity: ~0.51m/s

VC1.8m/min-SD160mm-*B850*

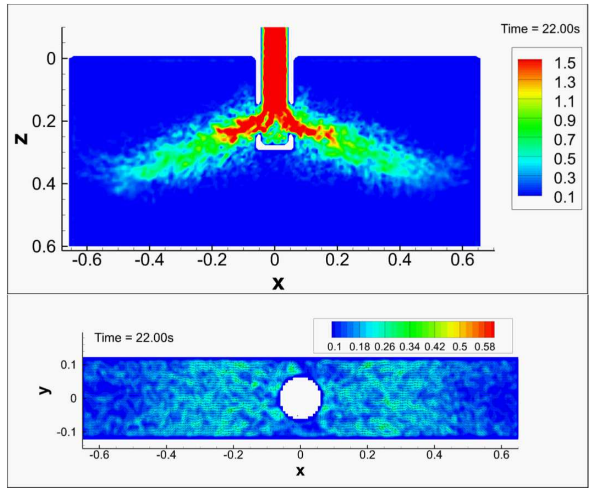

Time averaged Max top surface velocity: ~0.17m/s

Effect of EMBr on Time-Averaged flow in Mid and Top Surface (160mm Submergence, Vc = 1.8m/min) (Simulations 6 and 7)

- Time averaged result, casting speed 1.8m/min
- Contour of velocity magnitude (m/s)

No EMBr

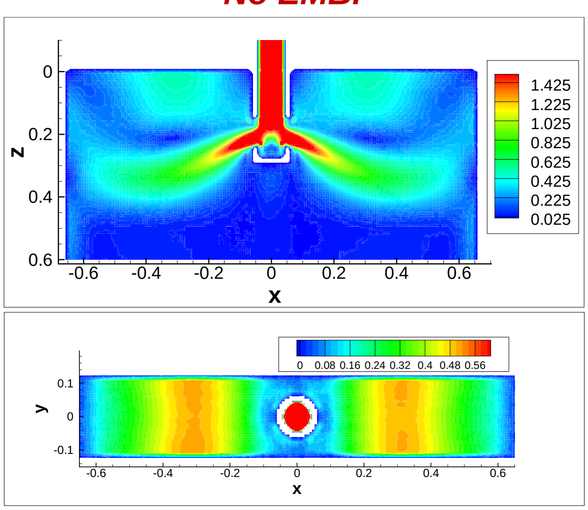

Max top surface velocity: ~0.51m/s

B850

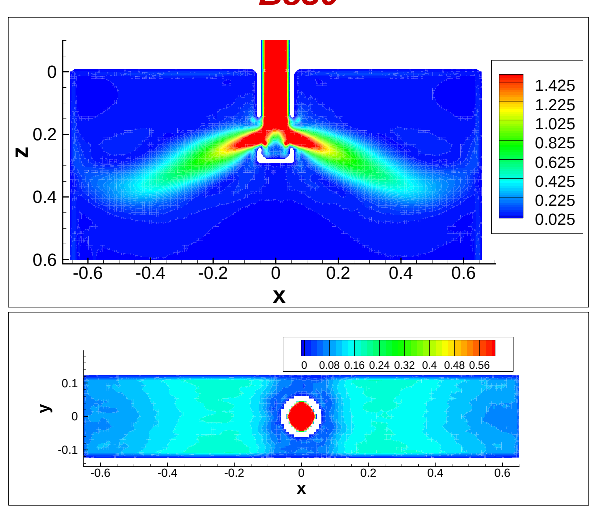

Max top surface velocity: ~0.17m/s

EMBr Effect on Flow Pattern

(160mm Submergence, Vc = 1.8m/min)
(Simulations 6 to 8)

- Stream lines and contours of velocity magnitude (m/s)
- EMBr lowers surface velocity and brings recirculation regions closer to the jet

No EMBr

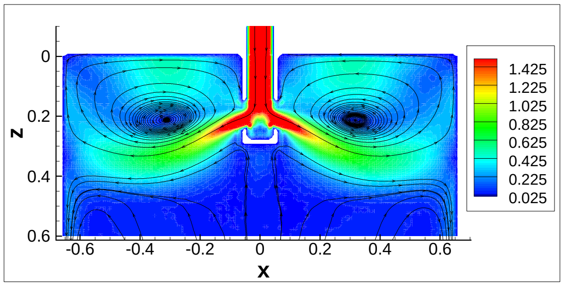

B850

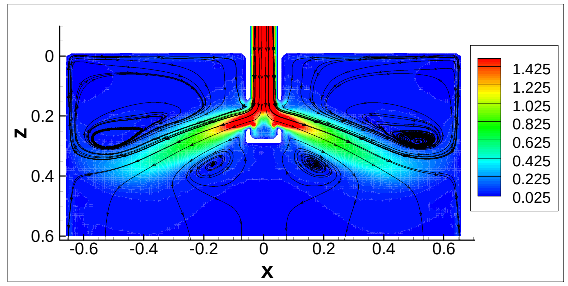

T400 / B600

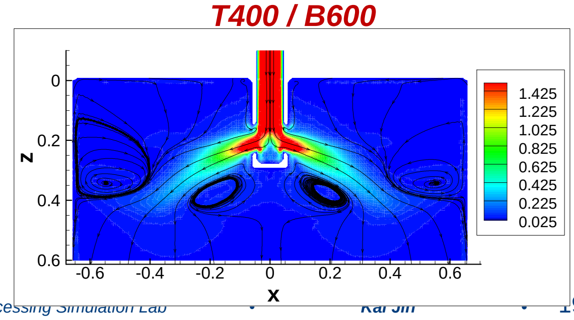

With magnetic field and this high casting speed, the lower recirculation zone shrinks to a small vortex below the jet. Agreed with previous LES simulations by R-Singh[1].

EMBr Effect on Flow Pattern in Top Surface (160mm Submergence, Vc = 1.8m/min) (Simulations 6 to 8)

- Top surface velocity contour (unit m/s)
- Only apply bottom EMBr (current 850A) reduce top surface velocity by ~67%, with both top and bottom EMBr (400A and 600A) reduce surface velocity by ~82%

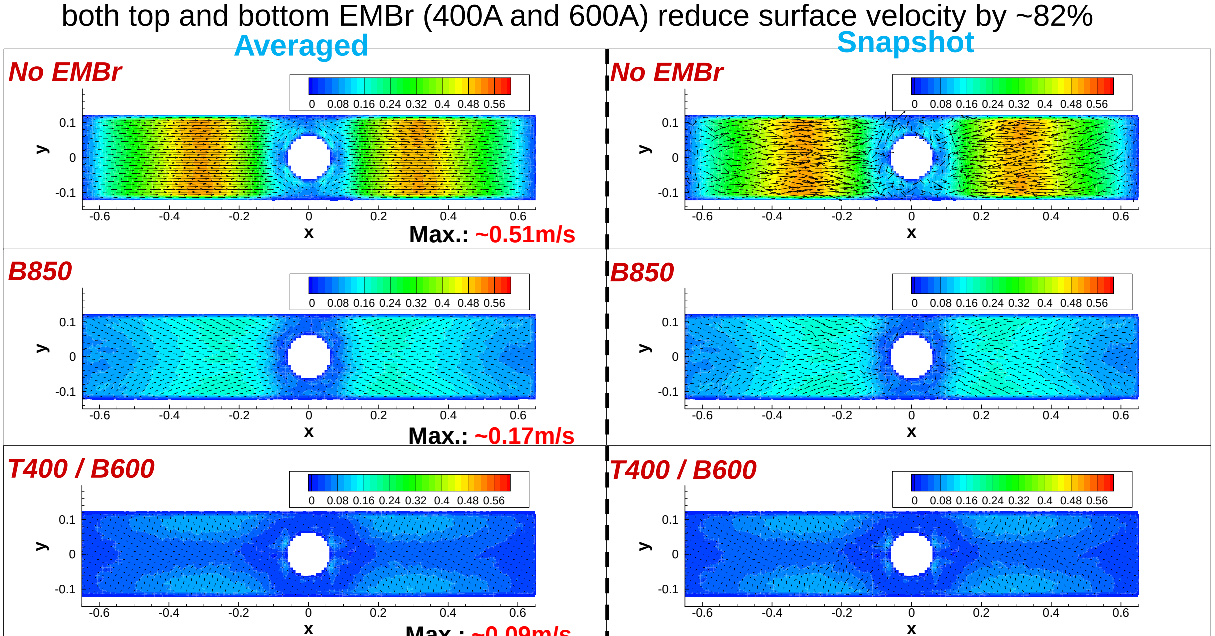

EMBr Effect on Level Fluctuation at Top Surface (160mm Submergence, Vc = 1.8m/min)

VC1.8m/min-SD160mm-*NoEMBr*

$$h = \frac{p - p_0}{\rho_L g}$$

p_0 is static pressure

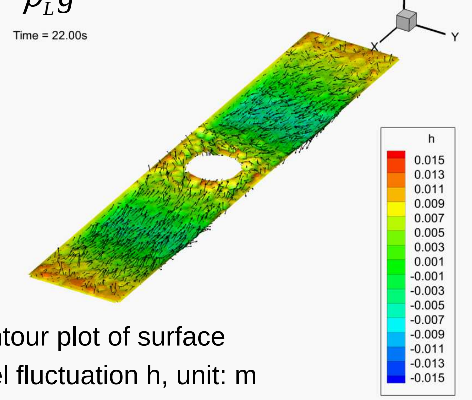

Contour plot of surface level fluctuation h, unit: m

VC1.8m/min-SD160mm-*B850*

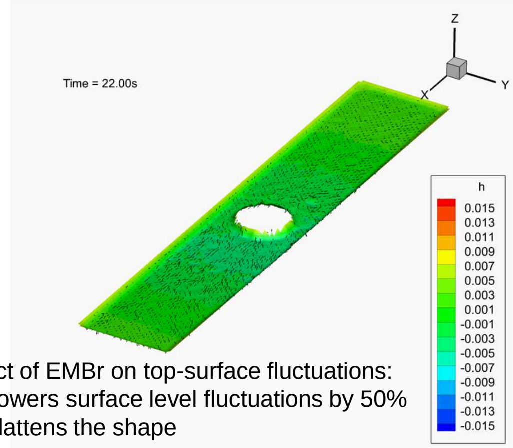

Effect of EMBr on top-surface fluctuations:
- lowers surface level fluctuations by 50%
- flattens the shape

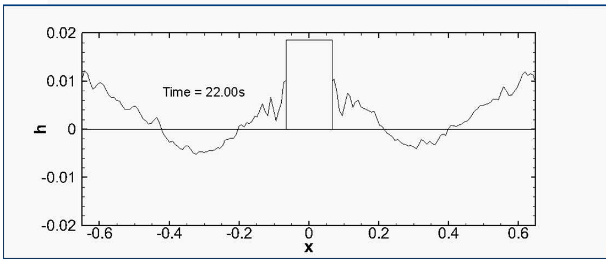

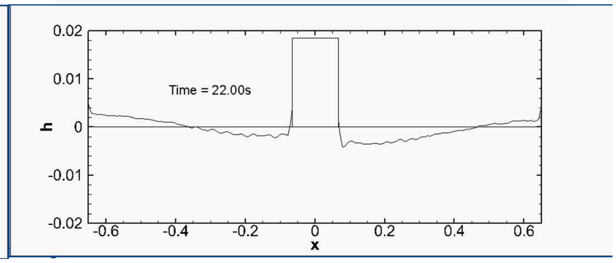

Pressure Fluctuations at 3 Different Points with *Vc = 1.5m/min* and submergence depth 160mm

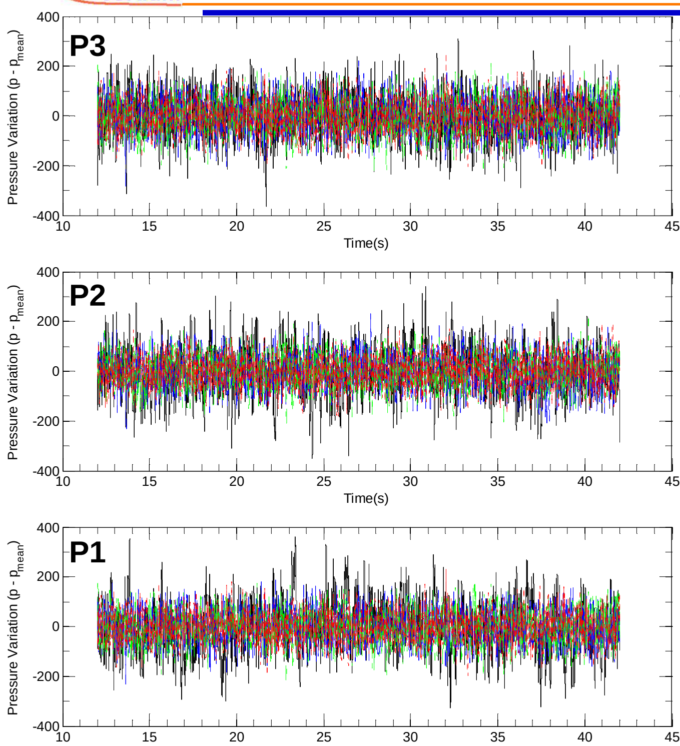

- EMBr reduce pressure fluctuations by 25%~40% at region 1cm below top surface
- More effective in reducing fluctuations at region far away from SEN;

VC15NOEMBR
VC15B600
VC15B850
VC15T400B600

$$s = \left(\frac{\sum_{i=1}^{n} (p_i - \bar{p})^2}{n-1} \right)^{\frac{1}{2}}$$

$$\bar{p} = \frac{1}{n} \sum_{i=1}^{n} p_i$$

$$n = 150000$$

EMBr	s of P3
No EMBr	82.5
B600	61.3
B850	60.3
T400B600	55.1

EMBr	s of P2
No EMBr	91.4
B600	57.0
B850	55.7
T400B600	50.9

EMBr	s of P1
No EMBr	97.0
B600	56.7
B850	55.6
T400B600	50.7

Locations of P1, P2, P3 (1cm below meniscus)

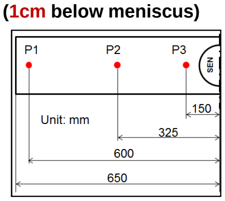

Pressure Fluctuations at 3 Different Points with *Vc = 1.8m/min* and submergence depth 160mm

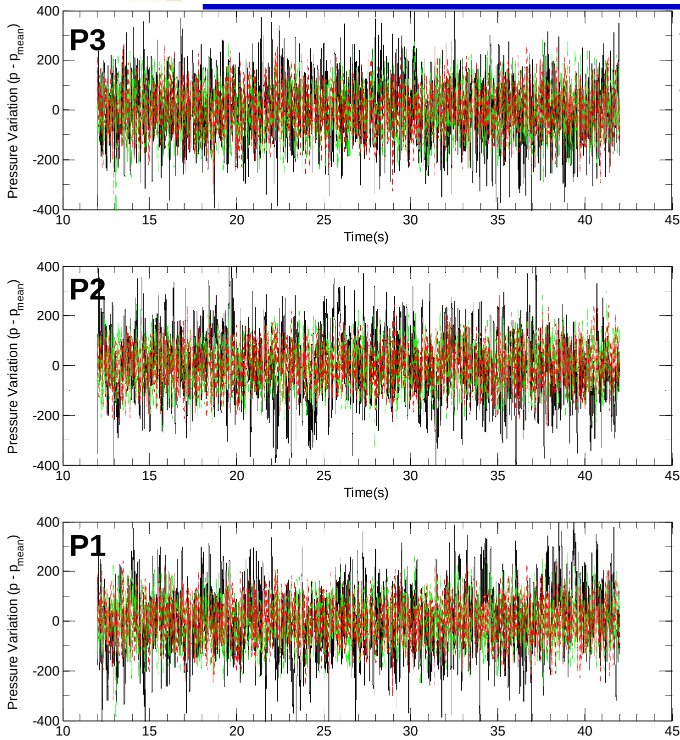

- Higher casting speed leads to higher fluctuations close to top-surface;
- EMBr reduce more fluctuations at region far away from SEN;

EMBr	s of P3
No EMBr	117.0
B850	84.0
T400B600	79.0

EMBr	s of P2
No EMBr	129.1
B850	76.3
T400B600	70.3

EMBr	s of P1
No EMBr	132.0
B850	76.3
T400B600	72.2

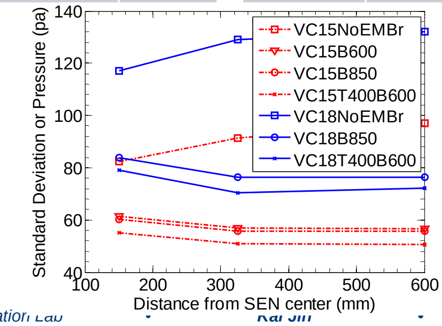

Conclusions of Part II

- With small submergence depth (160 and 210), increasing submergence depth increases surface velocity slightly, with ~same flow pattern;
- EMBr causes center of all 4 recirculation regions to move closer to the jet;
- Applying bottom-only B600 EMBr reduces top surface velocity by 60% (from ~0.45 to ~0.16m/s at 1.5m/min). Applying B850 makes flow too slow (0.??m/s).
- Applying bottom-only B850 EMBr reduces top surface velocity by ~70% (from ~0.6 to ~0.2m/s at 1.8m/min);
- For both casting speed 1.5 &1.8m/min, high strength top EMBr makes meniscus flow very small (less than 0.1m/s) and is likely not a good practice in operation;
- At higher casting speed (1.8m/min) applying only bottom EMBr lowers surface level fluctuations by 50% (from ~2cm to ~1cm) and flattens the shape as well.
- With Vc=1.8m/min and No EMBr, time-averaged max top-surface velocity is 0.51m/s, transient simulation shows at ¼ region of the top-surface velocity can be ~20% higher (~0.6m/s);
- Pressure fluctuations slightly below top surface show that w/o EMBr, region close to NF has larger pressure fluctuations. EMBr is more effective (about 2 times more effective) in suppressing fluctuations at region far away from SEN.

Part III & IV – Study of Effect of EMBr on Bubble Capture in Caster

Objectives

- Use advanced capture criterion to study the effect of EMBr on Ar gas bubble behavior: predict bubble trajectories and entrapment;
- Compare model prediction and measurements with EMBr (without EMBr was presented in 2013)
- Evaluate the distribution of captured particles, and provide suggestions on plant operation.

Casting Conditions

Two new Simulations (2 and 3)

	EMBr
1	No EMBr
2	Bottom coil current 600 A
3	Top coil current 400 A & Bottom coil current 600 A

Casting Conditions	Value
Mold Thickness	230 mm
Mold Width	1300 mm
Submergence Depth	160 mm
Port Downward Angle	15 deg.
Casting Speed	1.5 m/min
Ar injection	8.2% vol.

For each case, post-tracking release 0.24million bubbles, with random walk model. Then repeat 10 times (total 2.4 million particles are tracked for each case) and get averaged results.

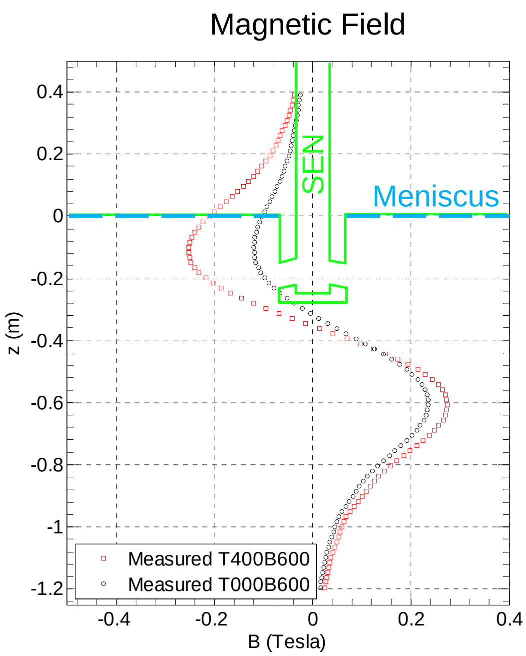

Geometry and Boundary Conditions

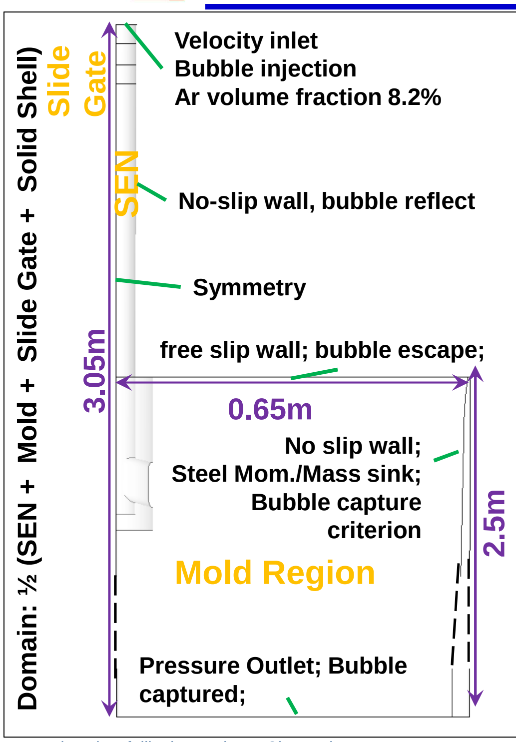

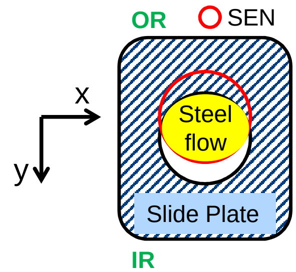

Steel first enter IR side of SEN

Location	Boundary Conditions
Inlet	V = 1.69 m/s; 8.2% vol. fraction of Ar
Outlet	pressure 184kpa; particle captured;
Sym. Plane	Symmetry;
Meniscus	free-slip wall; particle escape;
NF and WF	no-slip wall; steel mass & momentum sink; particle capture criterion UDF;
SEN Walls	no-slip wall; particle reflect;

Governing Equation For Fluid Flow Steel and Ar Properties

- Continuity Equation

$$\frac{\partial u_i}{\partial x_i} = 0$$

- Steel momentum equation

$$\frac{\partial u_i}{\partial t} + u_j \frac{\partial u_i}{\partial x_j} = -\frac{1}{\rho}\frac{\partial p}{\partial x_i} + \nu \frac{\partial u_i}{\partial x_j x_j} + F_i$$

Properties	Steel	Ar
Density (kg/m³)	7,000	0.5
Viscosity (kg/m-s)	0.0063	2.12e-5

- Steady-State RANS Turbulence Model (*k*-*ε*)

$$\frac{\partial}{\partial t}(\rho k) + \frac{\partial}{\partial x_i}(\rho k u_i) = \frac{\partial}{\partial x_j}\left[\left(\mu + \frac{\mu_t}{\sigma_k}\right)\frac{\partial k}{\partial x_j}\right] - \rho\overline{u'_i u'_j}\frac{\partial u_j}{\partial x_i} - \rho\epsilon; \qquad \mu_t = \rho C_\mu \frac{k^2}{\epsilon}$$

$$\frac{\partial}{\partial t}(\rho \epsilon) + \frac{\partial}{\partial x_i}(\rho \epsilon u_i) = \frac{\partial}{\partial x_j}\left[\left(\mu + \frac{\mu_t}{\sigma_\epsilon}\right)\frac{\partial \epsilon}{\partial x_j}\right] + C_{1\epsilon}\frac{\epsilon}{k}\left(\rho\overline{u'_i u'_j}\frac{\partial u_j}{\partial x_i}\right) - C_{2\epsilon}\rho\frac{\epsilon^2}{k}$$

$$C_{1\epsilon} = 1.44; \quad C_{2\epsilon} = 1.92; \quad C_\mu = 0.09; \quad \sigma_k = 1.0; \quad \sigma_\epsilon = 1.3$$

$$\rho\overline{u'_i u'_j}\frac{\partial u_j}{\partial x_i} = \mu_t\left(\nabla\vec{u} + (\nabla\vec{u})^T\right) : \nabla\vec{u}$$

$\vec{u}$ Steel velocity
$\vec{g}$ Gravity
ρ Steel density
$\vec{F}$ Sorce term
μ Steel dynamic viscosity
k Turbulent kinetic energy
ε Turbulent dissipation rate

Particle Tracking with Random Walk Model

Equation of Motion for Particles

$$\frac{d\vec{u}_p}{dt} = F_D\left(\vec{u}-\vec{u}_p\right) + \frac{\vec{g}\left(\rho_p-\rho\right)}{\rho_p} + \vec{F}_s$$

$$\mathrm{Re}_p = \frac{\rho d_p\left|\vec{u}_p-\vec{u}\right|}{\mu}$$

$$F_D = \frac{18\mu}{\rho_p d_p^{\,2}}\frac{C_D \mathrm{Re}_p}{24}$$

Spherical drag law suggested by S. A. Morsi and A. J. Alexander

↓

$$C_D = a_1 + \frac{a_2}{\mathrm{Re}_p} + \frac{a_3}{\mathrm{Re}_p^{\,2}}$$

$$a_1,a_2,a_3 = \begin{cases} 0, 24, 0 & 0<\mathrm{Re}_p<0.1 \\ 3.690, 22.73, 0.0903 & 0.1<\mathrm{Re}_p<1 \\ 1.222, 29.1667, -3.8889 & 1<\mathrm{Re}_p<10 \\ 0.6167, 46.50, -116.67 & 10<\mathrm{Re}_p<100 \\ 0.3644, 98.33, -2778 & 100<\mathrm{Re}_p<1000 \\ 0.357, 148.62, -47500 & 1000<\mathrm{Re}_p<5000 \\ 0.46, -490.546, 578700 & 5000<\mathrm{Re}_p<10000 \\ 0.5191, -1662.5, 5416700 & \mathrm{Re}_p>10000 \end{cases}$$

$\vec{u}_p$	Particle velocity
$\vec{u}$	Steel velocity
F_D	Drag force
$\vec{g}$	Gravity
ρ_p	Particle density
ρ	Steel density
$\vec{F}_s$	Sorce term
μ	Steel dynamic viscosity
d_p	Paticle diameter
C_D	Drag coefficient
Re_p	Particle Reynolds number
t_e	Eddy life time
τ	Particle relaxation time
t_{cross}	Eddy cross time
T_L	Fluid Lagrangian integral time
C_μ	Constant in k-ε model, 0.09
k	Turbulent kinetic energy
ε	Turbulent dissipation rate
$\dot{m}_p$	particle stream mass flow rate

Momentum Exchange to Fluid

$$\vec{F} = \sum\left(\frac{18\mu}{\rho_p d_p^{\,2}}\frac{C_D \mathrm{Re}_p}{24}\left(\vec{u}_p-\vec{u}\right)\right)\dot{m}_p\Delta t$$

Discrete Random Walk Model

Gaussian distributed random velocity fluctuation, *u'*, *v'* and *w'* are generated from

$$u' = \zeta\sqrt{\overline{u'^2}} \qquad \sqrt{\overline{u'^2}} = \sqrt{\overline{v'^2}} = \sqrt{\overline{w'^2}} = \sqrt{2k/3}$$

ζ – standard normal distribution random number.

$$t_L = C_L\frac{k}{\epsilon} \approx 0.15\frac{k}{\epsilon} \qquad t_e = -t_L\ln(r)$$

$$\tau = \frac{\rho_p d_p^{\,2}}{18\mu} \qquad t_{cross} = -\tau\ln\left[1-\frac{C_\mu^{4/3}\frac{k^{3/2}}{\epsilon}}{\tau\left|\vec{u}-\vec{u}_p\right|}\right]$$

r – uniformly distributed random number from 0 and 1. This yields a random eddy life time.

use k, ε and ζ to calculate fluctuations

↓

evaluate t_e and t_{cross}

↓

interaction time t_{inter} = $min(t_e, t_{cross})$

↓

interaction time reached?

Yes → new ζ → use k, ε and ζ to calculate fluctuations

No → use k, ε and ζ to calculate fluctuations

Bubble Distribution

As stated before, there are 2 Steps in the simulation:

- **Step-1: Two-way coupled Eulerian-Lagrangian simulation to obtain fluid field;**
- **Step-2: Particles are randomly released from inlet; trajectories are tracked by Random Walk Model.**

Diameter of injected bubble and their volume fraction

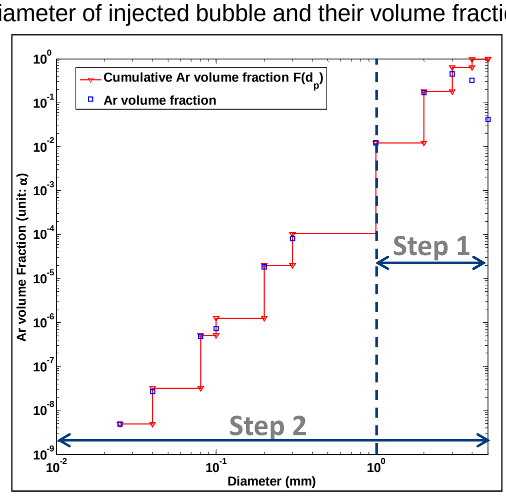

Note:
More details about mesh, equations, validation and comparison of capture criterion can be found in my 2013 CCC meeting slides[2].

The distribution of Injected bubbles satisfies Rosin-Rammler distribution, with mean diameter 3mm.

In step – 1, two-way coupled simulation with 5 different groups of bubbles

In step – 2, 10 different groups of bubbles are injected and tracked.

244,239 bubbles are injected in total

α is total Ar volume fraction at injection point whish is 8.2% vol in this case.

Capture Criterion

- **Advanced capture criterion** is implemented and the criterion is described both in Quan Yuan's PhD thesis (2004) [3], Sana Mahmood's Master thesis (2006) [4] and Thomas, Brian G., et al [5]. A flow chart of capture criterion is given in figure below.

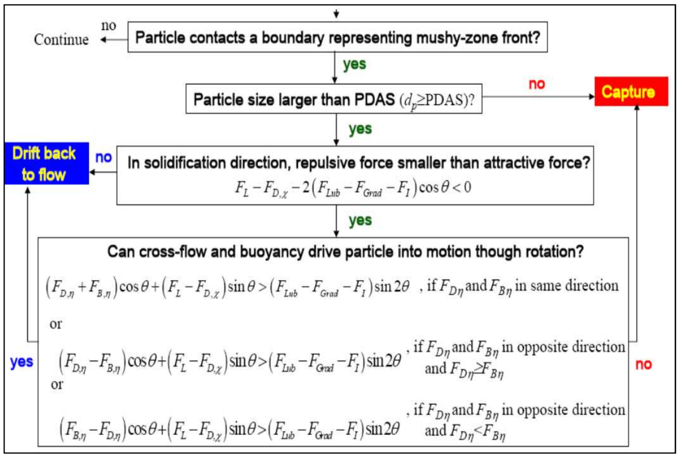

Advanced Capture Criterion (Figure from Sana Mahmood, Master thesis, 2006[3])

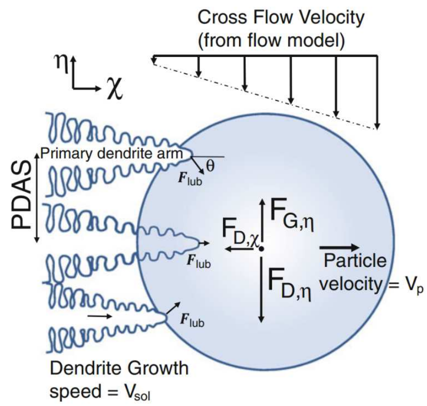

A Bubble/Particle Touching 3 Dendrite Tips (Figure from Thomas, Brian G., et al [5])

Forces Related to Capture Criterion

R_p particle radius

V_{sol} solidification velocity

r_d dendrite tip radius

h_o distance between dendrite tip and particle

a_o atomic diameter of the liquid

C_o sulfur content of steel

D_s diffusion coefficient of sulfur in steel

k distribution coefficient

Theoretical solidification velocity is used on NF/WF

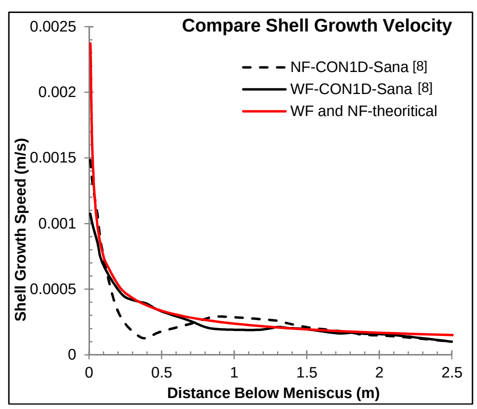

Forces on particles [5,6]:

$$F_B = (\rho_{steel} - \rho_{Ar}) g \frac{4}{3}\pi R_p^3$$

Buoyancy force pointing upward

$$F_{lub} = 6\pi\mu V_{sol} \frac{R_p^2}{h_o}\left(\frac{r_d}{r_d + R_p}\right)^2$$

Lubrication force acts on the particle along particle's radius towards dendrite tip

$$F_I = 2\pi\Delta\sigma_o \frac{r_d R_p}{r_d + R_p}\frac{a_o^2}{h_o^2} \qquad \Delta\sigma_o = \sigma_{sp} - \sigma_{sl} - \sigma_{pl}$$

Van der Waals force pushes particle away from dendrite tip

$$F_{Grad} = -\frac{m\beta\pi R_p}{\xi^2}\left\{\frac{\xi^2 - R_p^2}{\beta}\ln\frac{(\xi + R_p)[\alpha(\xi - R_p) + \beta]}{(\xi - R_p)[\alpha(\xi + R_p) + \beta]}\right\} + \frac{2R_p}{\alpha} - \frac{\beta}{\alpha^2}\ln\frac{\alpha(\xi - R_p) + \beta}{\alpha(\xi + R_p) + \beta}$$

Interfacial gradient force push particle toward solidification front

$$\alpha = 1 + nC_o$$
$$\beta = nr_d(C^* - C_o)$$
$$\xi = R_p + r_d + h_o$$
$$\frac{r_d V_{sol}}{2D_s} = \frac{C^* - C_o}{C^*(1-k)}$$

Relate Bubble Capture Prediction with Measurement

- Which bubble can be found in a certain slice of a sample, e.g. x_s=9mm?

Need to satisfy: $x_i<x_s$ and $x_i+r_i>x_s$ or $x_i>x_s$ and $x_i-r_i<x_s$

Sample from Measurement

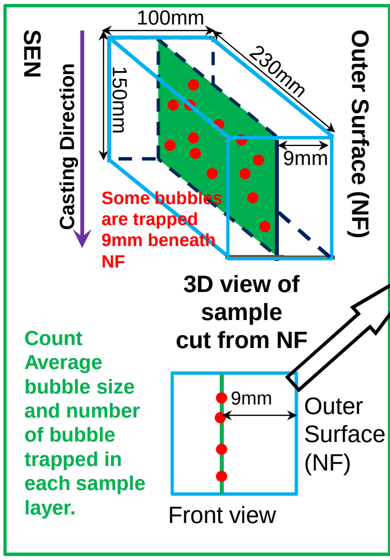

Bubbles/Particles Captured in Simulation

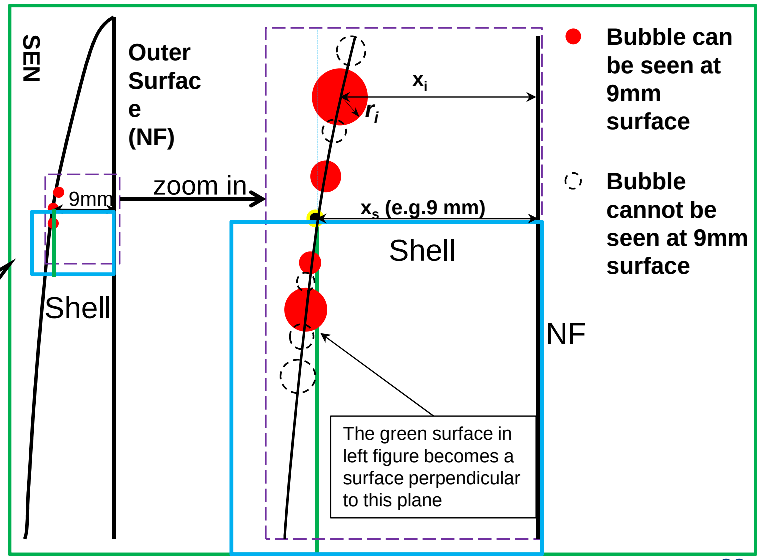

Method to Predict Number of bubbles Captured in a Slice of Sample

Task: Predict the number of bubbles captured (n) by a slice that is x_s beneath a NF sample which has length L in casting direction. Then find if L is changed to L', what the number (n') will be?

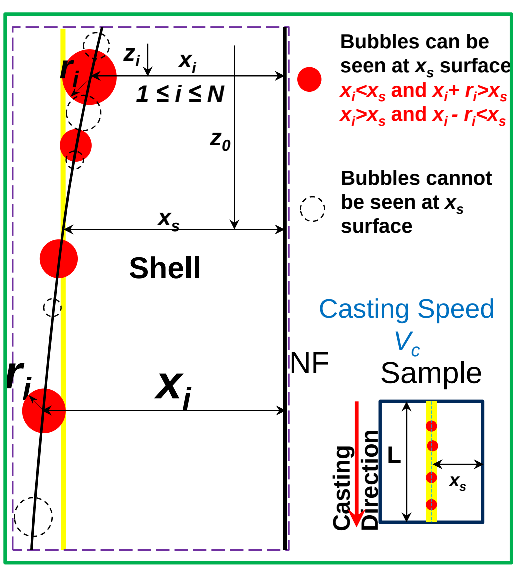

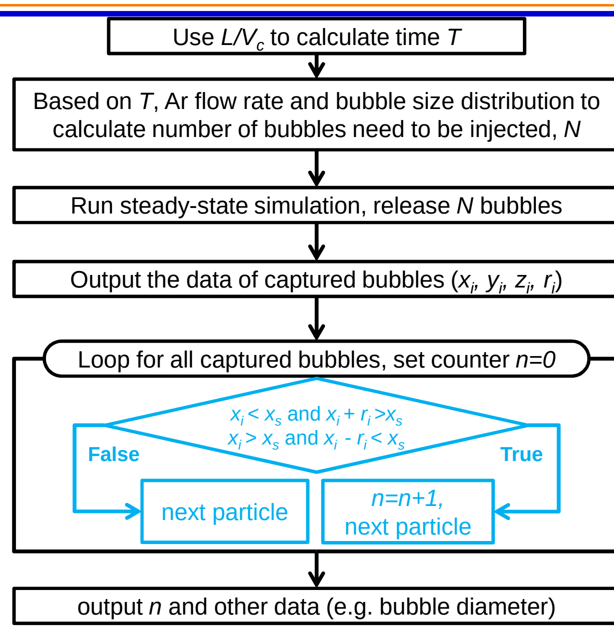

n/L – number of particles captured per unit length (unit: particle/mm). This can be used even the sample size is changed: $n' = n/L*L'$

Flow Field with EMBr and Ar Gas

- Contour plot of velocity magnitude (m/s)

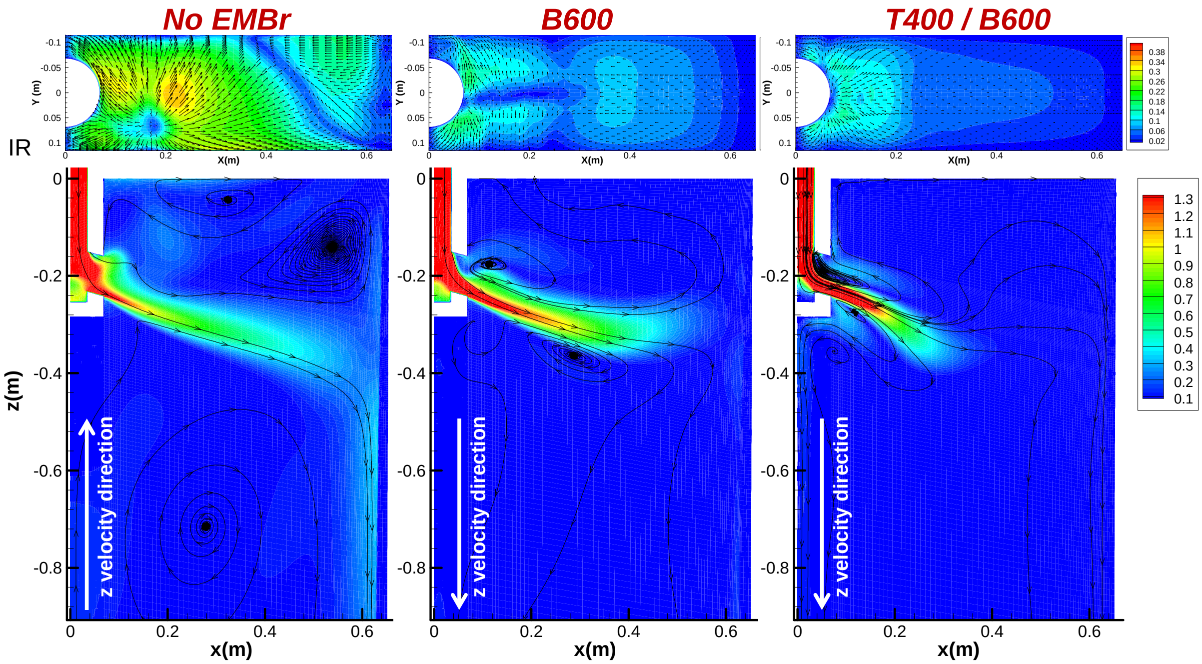

Small-bubble distributions with No EMBr (Diameter ≤ 0.3mm)

- Slide gate open to IR, more capture on IR due to more gas escape from IR side;

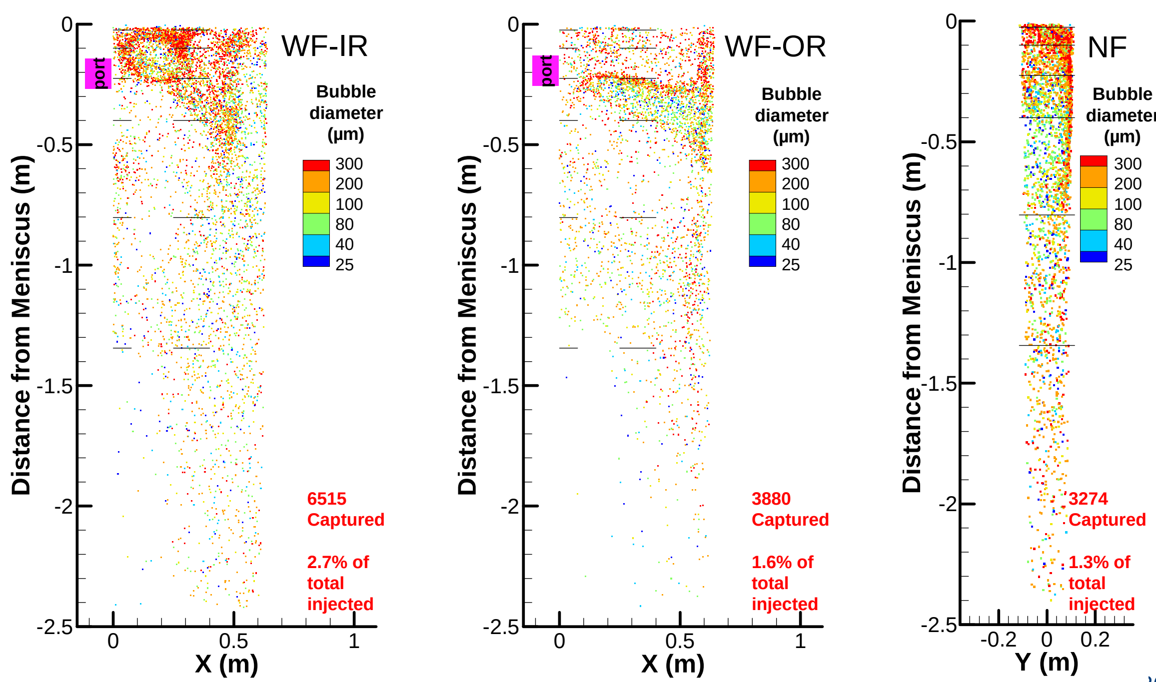

Small-bubble distributions with B600 EMBr (Diameter ≤ 0.3mm)

- With B600 EMBr, capture on IR and OR are more similar;
- With B600 EMBr, number of bubbles captured by NF is reduced by 48% compare with no EMBr;

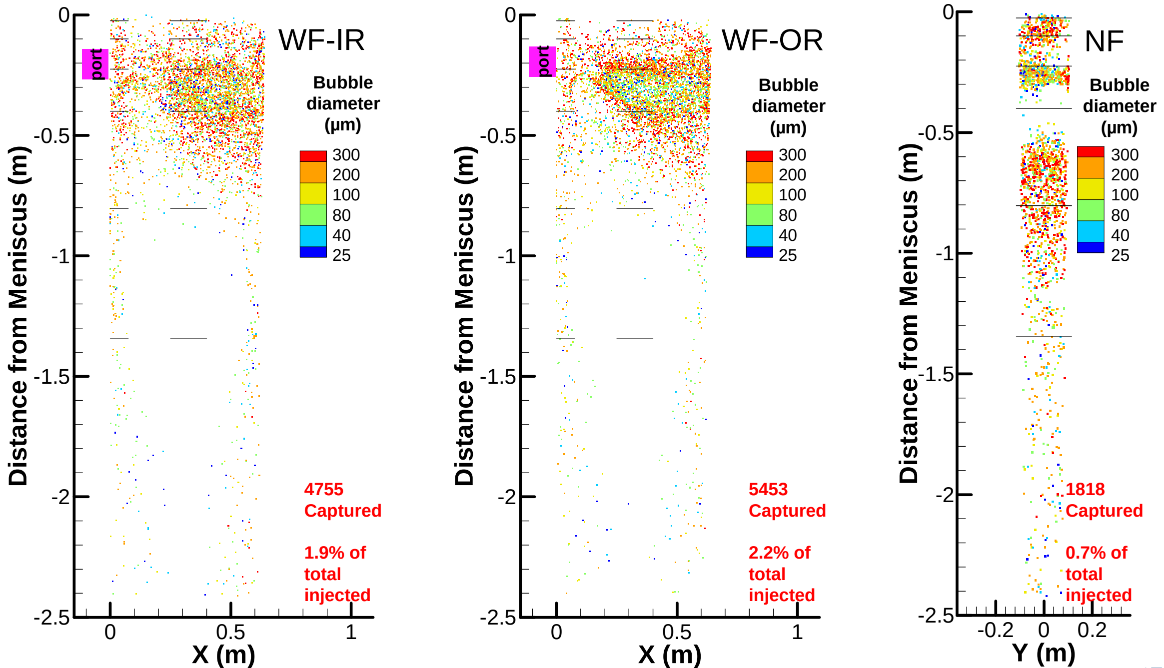

Small-bubble distributions with T400 / B600 EMBr (Diameter ≤ 0.3mm)

- With T400 / B600 EMBr, capture on IR and OR looks very same
- With T400 / B600 EMBr, number of bubbles captured by NF is reduced by ~75% compare with no EMBr;

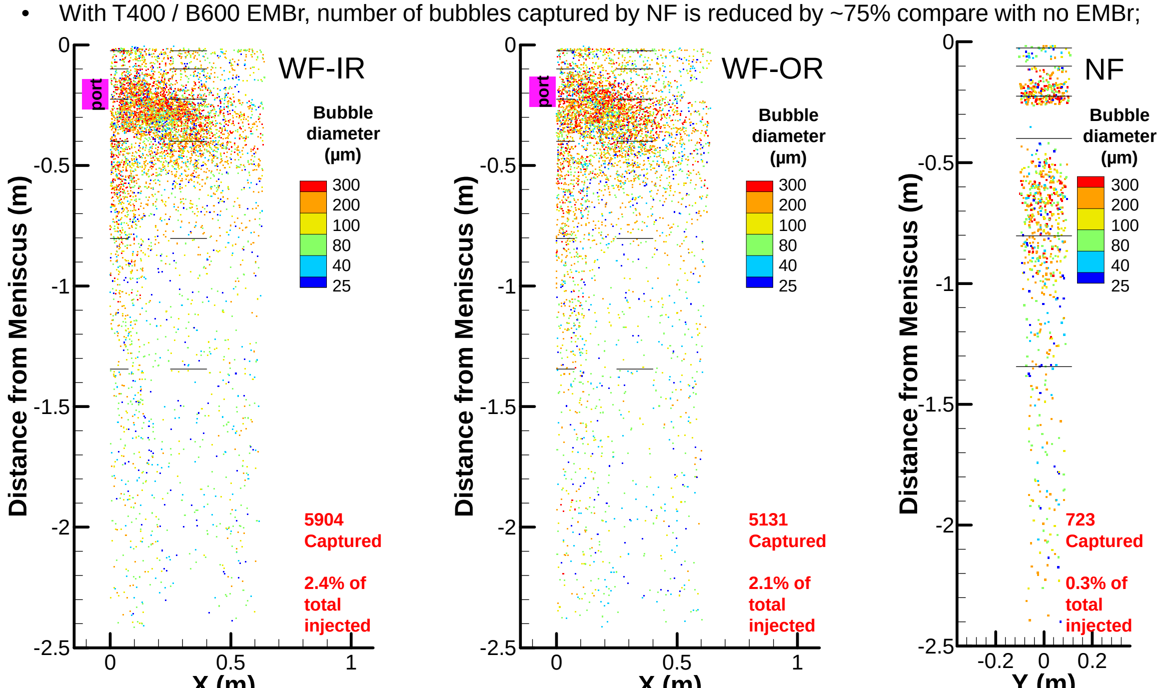

Large-Bubble Distributions with No EMBr (Diameter ≥1mm)

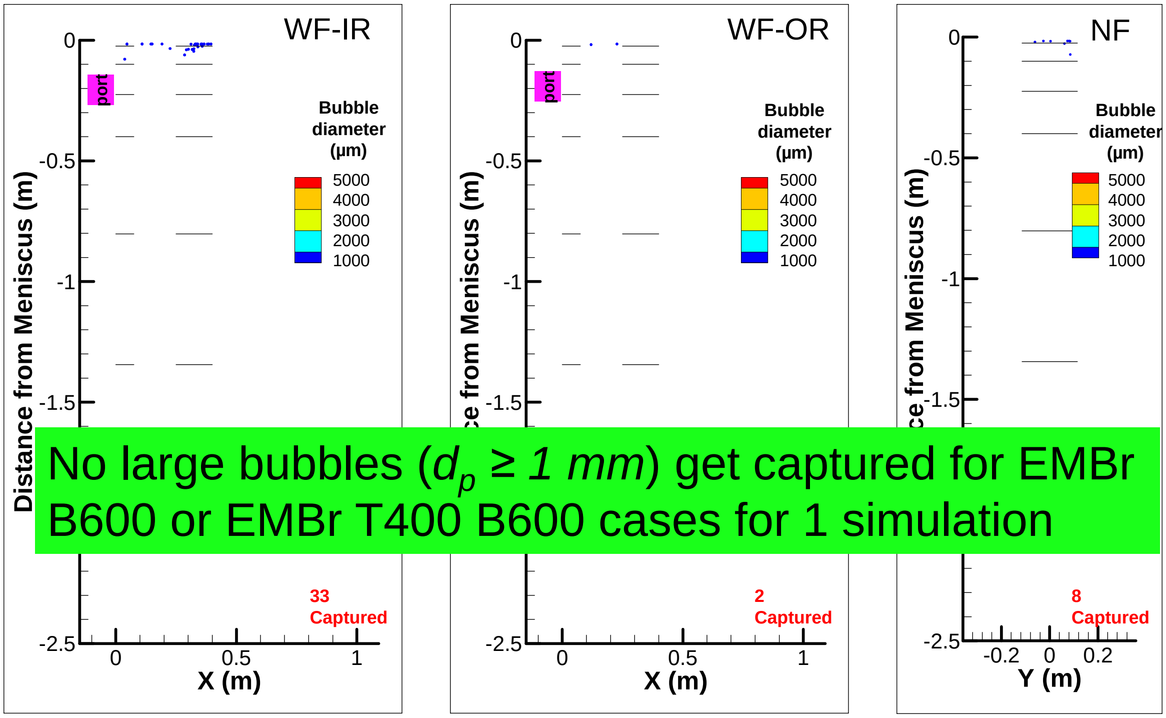

No large bubbles (d_p ≥ *1 mm*) get captured for EMBr B600 or EMBr T400 B600 cases for 1 simulation

Effect of EMBr on Bubble Capture (Average Number of Captured Bubble)

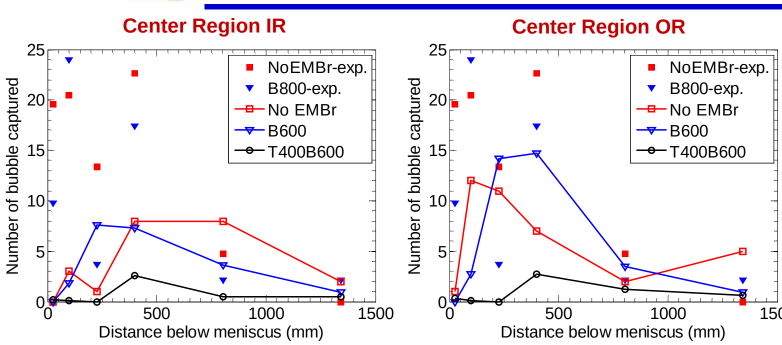

- 6 locations below meniscus associated with 3, 6, 9, 12, 17, 22 mm from out surface of the slab.
- Simulations predict less particles captured close to meniscus, because hook is not in the model.

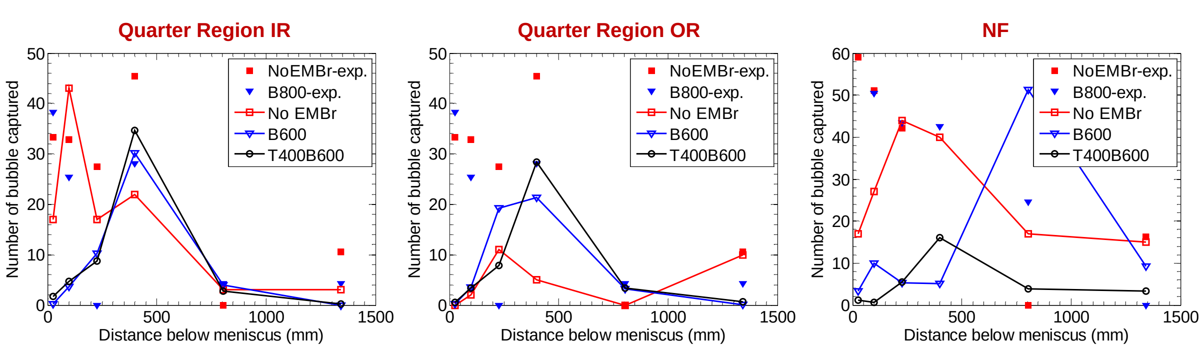

Effect of EMBr on Bubble Capture (Average Bubble Diameter)

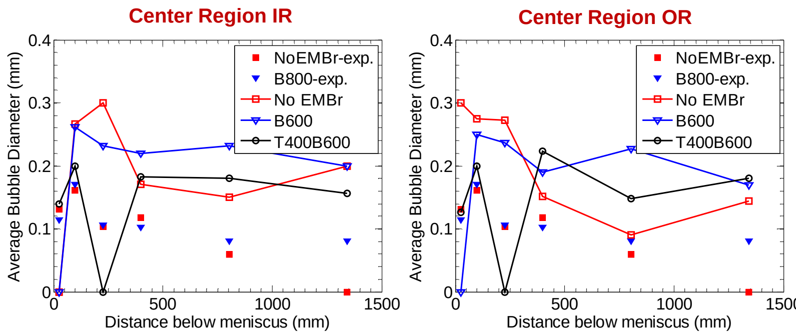

- 6 locations below meniscus associated with 3, 6, 9, 12, 17, 22 mm from out surface of the slab.
- Simulations always predict larger particle diameter, this may due to the injected bubbles are larger than that of bubbles in real caster.

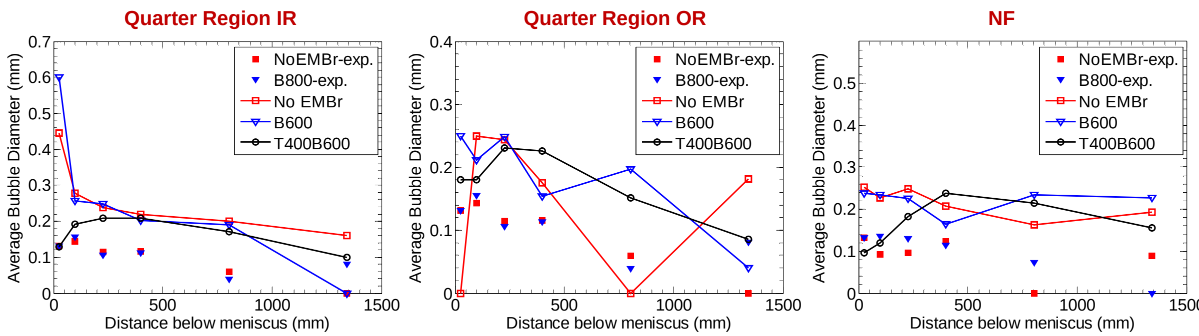

Part IV: Effect of EMBr on Bubble Capture

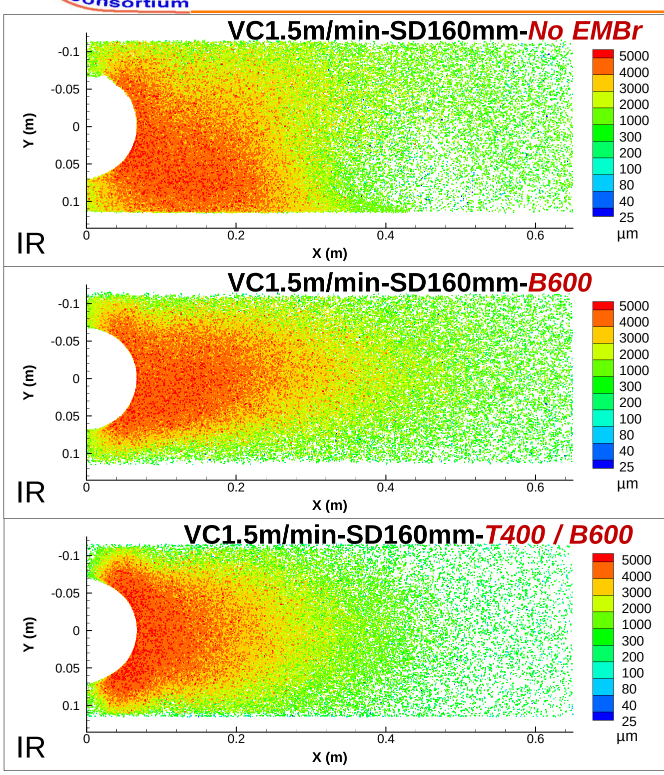

Bubbles Escaped from Meniscus
(Colored by bubble diameter)

- EMBr makes bubble escape from the middle region of top surface, less bias escaping of bubbles;
- Stronger EMBr make more bubbles escape from region close to SEN

Effect of EMBr on Bubble Capture Rates and Fractions

- Bubble capture rates and fractions (averaged of 10 simulations for each case);
- EMBr has less effect on capture rates of small bubbles;
- Capture rate for small bubbles ($d_p \leq 0.1$mm) is almost the same (~70%);
- Large bubbles has very low capture fraction (<0.1%); especially with EMBr (<0.002%)

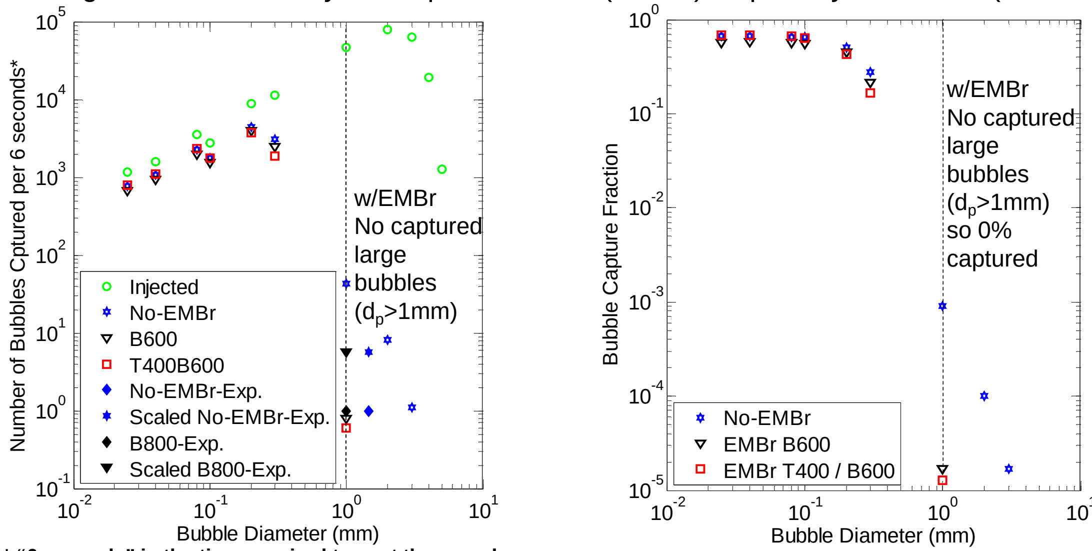

*** “6 seconds” is the time required to cast the sample**

Conclusions of Part III and IV

- Current simulations predict the same trend of captured bubble diameter but the predicted average diameter is larger than measured. This may due to the assumed distribution of bubble size (mean 3mm and Rosin-Rammler distribution) may larger than that in real caster;
- Although advanced capture model is much better than simple capture model[2], bubble capture near the meniscus (strand surface) is still under-predicted, perhaps because hooks are not included in the model;
- Magnetic field causes more symmetrical flow distribution and bubble escape to the top surface. Without EMBr, there is significant surface cross flow from IR to OR, (due to slide gate opening towards IR causing Ar gas flow asymmetry), leading to more bubble capture on IR[2]);
- Magnetic field reduces the bubble capture rate on NF and makes more uniform capture on WF IR and OR,
- Capture rates on WF and NF are very similar (per unit area).
- Capture rates for small bubbles are MUCH larger then that of large bubbles and for bubbles less then 0.1mm the capture fraction are almost the same (~70%); large bubbles are very rarely captured even without EMBr(<0.1%);
- EMBr lowers capture rate for 1mm bubbles (from 0.1% to 0.002%)
- Larger bubbles are rarely captured;

Future Work

- Investigate the average size and distribution of Ar gas bubbles in mold and investigate a more realistic bubble distribution which can be used in future;
- Add hook capture mechanism into the advanced capture criterion and implement it into Fluent/CUFLOW.
- Implement two-way fluid and particle interaction and capture criterion into multi-GPU CUFLOW and use transient LES simulations to study the capture of bubbles/particles;

Acknowledgments

- Continuous Casting Consortium Members (ABB, ArcelorMittal, Baosteel, Magnesita Refractories, Nippon Steel and Sumitomo Metal Corp., Nucor Steel, Postech/ Posco, Severstal, SSAB, Tata Steel, ANSYS/ Fluent)
- Blue Waters / National Center for Supercomputing Applications (NCSA) at UIUC
- National Science Foundation Grant CMMI-11-30882
- NVIDIA for providing the GPU cards through the NVIDIA Professor Partnership program

Reference

[1] Singh, Ramnik, Brian G. Thomas, and Surya P. Vanka. "Large Eddy Simulations of Double-Ruler Electromagnetic Field Effect on Transient Flow During Continuous Casting." *Metallurgical and Materials Transactions B* 45.3 (2014): 1098-1115.

[2] Kai Jin, “07_JIN-K_Mltiphase_Flow_EMBr_Bubble_Entrapment.pptx”, CCC Annual Meeting slides, 2013, UIUC

[3] Quan Yuan, "*Transient Study of Turbulent Flow and Particle Transport during Continuous Casting of Steel Slabs*," PhD Thesis, University of Illinois, June, 2004.

[4] Sana Mahmood, “*Modeling of Flow Asymmetries and Particle Entrapment in Nozzle and Mold During Continuous Casting of Steel Slabs*”, MS Thesis, University of Illinois, 2006

[5] Thomas, Brian G., et al. "Transport and Entrapment of Particles in Steel Continuous Casting." *Metallurgical and Materials Transactions B* 45.1 (2014): 22-35.